IEEE Access
Multidisciplinary ⋮ Rapid Review ⋮ Open Access Journal

Received 17 January 2023, accepted 7 February 2023, date of publication 10 February 2023, date of current version 15 February 2023.

Digital Object Identifier 10.1109/ACCESS.2023.3244119

RESEARCH ARTICLE

CMA-Based Quadruple-Cluster Leaf-Shaped Metasurface-Based Wideband Circularly-Polarized Stacked-Patch Antenna Array for Sub-6 GHz 5G Applications

NATHAPAT SUPREEYATITIKUL[1], (Member, IEEE), PISIT JANPANGNGERN[2], TITIPONG LERTWIRIYAPRAPA[3], (Senior Member, IEEE), MONAI KRAIRIKSH[2], (Senior Member, IEEE), AND CHUWONG PHONGCHAROENPANICH[2], (Member, IEEE)

[1]Aeronautical Engineering Division, Civil Aviation Training Center, Bangkok 10900, Thailand
[2]School of Engineering, King Mongkut's Institute of Technology Ladkrabang, Bangkok 10520, Thailand
[3]Research Center of Innovation Digital and Electromagnetic Technology (iDEMT), Department of Teacher Training in Electrical Engineering, Faculty of Technical Education, King Mongkut's University of Technology North Bangkok, Bangkok 10800, Thailand

Corresponding author: Chuwong Phongcharoenpanich (chuwong.ph@kmitl.ac.th)

This work was supported in part by the Royal Golden Jubilee Ph.D. Programme of the Thailand Research Fund (RGJ-TRF) under Grant PHD/0170/2560, in part by the National Science, Research and Innovation Fund (NSRF), and in part by the King Mongkut's University of Technology North Bangkok under Contract KMUTNB-FF-66-48.

ABSTRACT This research proposes a quadruple-cluster leaf-shaped metasurface (MTS)-based circularly-polarized (CP) stacked-patch antenna array with hybrid coupler feed network for sub-6 GHz 5G applications. In the study, the leaf-shaped MTS-based CP stacked-patch antenna is characterized by characteristic mode analysis (CMA). In the antenna design, one cluster of the quadruple-cluster leaf-shaped MTS-based antenna array consists of 4 × 4 leaf-shaped MTS elements; and the hybrid coupler feed network is used to enhance impedance bandwidth (IBW), axial ratio bandwidth (ARBW), and antenna gain. Simulations are carried out and an antenna prototype is fabricated and experiments undertaken. The measured IBW, ARBW, and maximum gain at the center frequency (4 GHz) are 62.5% (3.4 – 5.9 GHz), 21% (3.8 – 4.54 GHz), and 9.04 dBic at 3.9 GHz. The novelty of this research lies in the use of: (i) the CMA concept to design and develop the leaf-shaped wideband MTS-based stacked-patch antenna with CP radiation pattern; and (ii) a low-complexity hybrid coupler feed network to enhance the IBW, ARBW and gain.

INDEX TERMS Antenna arrays, characteristic mode analysis, couplers, metasurfaces, wideband.

I. INTRODUCTION

The fifth generation (5G) wireless communication technology is increasingly adopted for mobile wireless systems and the Internet of Things (IoT). The advantages of the 5G technology include high throughput, high channel capacity, and low latency [1]. The standard 5G spectrum is classified into three frequency bands: low-band (below 1 GHz), mid-band (below 6 GHz or sub-6 GHz), and high-band (above 24 GHz or mmWave) [2].

Of particular interest is the sub-6 GHz frequency band (1 – 6 GHz) which is widely adopted for commercial mobile broadband networks due to higher throughput, in comparison with the low-band frequency spectrum. Besides, the sub-6 GHz frequency spectrum achieves higher penetrability than the high-band frequency spectrum. Meanwhile, the commercial licenses of the sub-6 GHz 5G spectrum vary from country to country, i.e., in the USA (3.4 – 3.5 and

The associate editor coordinating the review of this manuscript and approving it for publication was Hassan Tariq Chattha.

3.7 – 4.2 GHz), the UK (3.8 – 4.2 GHz), China (3.3 – 3.6 and 4.5 – 5 GHz), and Japan (3.6 – 4.2 and 4.4 – 4.9 GHz) [3].

Circularly polarized (CP) antennas are used to transmit and receive signals in an interferent environment since the CP antennas are less susceptible to fading environments, multi-path distortions, and immune interference [4]. In [5], [6], [7], [8], [9], [10], [11], and [12], various types of CP antenna for 5G applications have been proposed. Specifically, in [5], a series slot-fed CP antenna achieves an impedance bandwidth (IBW) of 10.89% (27.2 – 30.35 GHz) and axial ratio bandwidth (ARBW) of 8.57% (27.3 – 29.7 GHz). In [6], a slanted stair-shaped dielectric resonator CP antenna achieves an IBW of 31% (4.9 – 6.7 GHz) and 3-dB ARBW of 18.2% (5 – 6 GHz).

In [7], a 4 × 4 dipole with hexagonal-shaped parasitic patches CP antenna array achieves an IBW of 27.7% (26.26 – 34.71 GHz) and 3-dB ARBW of 28.5% (27 – 36 GHz). In [8], a magnetoelectric dipole CP antenna achieves an IBW of 27.2% (4.77 – 6.27 GHz) and 3-dB ARBW of 42.3% (4.1 – 6.3 GHz). In [9], a meandering probe-fed CP patch antenna achieves an IBW of 27.2% (4.77 – 6.27 GHz) and 3-dB ARBW of 16.86% (5.05 – 5.98 GHz). In [10], a magnetoelectric dipole CP antenna using split-ring resonator lens achieves an IBW of 22.05% (29.5 – 37 GHz) and 3-dB ARBW of 7.35% (32.5 – 35 GHz).

Metasurface (MTS)-based structures are increasingly adopted in the design of CP antennas (i.e., MTS-based CP antennas) due to low complexity and low cost. The MTS structures are also utilized to improve impedance bandwidth and axial ratio bandwidth. In [11], a magneto-electric dipole CP antenna achieves an IBW of 13% (6.15 – 7.01 GHz) and 3-dB ARBW of 2.53% (6.24 – 6.4 GHz). In [12], a substrate integrated waveguide-fed CP antenna with parasitic patches achieves an IBW of 21% (5.37 – 6.95 GHz) and 3-dB ARBW of 7.35% (5.97 – 6.6 GHz). In [13], an S-shaped MTS-based CP antenna achieves an IBW of 43.22% (4.05 – 6.6 GHz) and 3-dB ARBW of 22% (5.3 – 6.6 GHz). In [14], a quadri-cluster CP sequentially-rotated MTS-based antenna array achieves an IBW of 84.74% (4 – 9 GHz) and 3-dB ARBW of 57.6% (4.2 – 7.6 GHz). In [15], a Z-shaped MTS-based CP fabry–pérot antenna achieves an IBW of 64% (4.4 – 7.6 GHz) and 3-dB ARBW of 18% (4.4 – 5.3 GHz). In [16], a staircase-shaped MTS-based CP antenna achieves an IBW of 67.3% (4.1 – 7.6 GHz) and 3-dB ARBW of 15.9% (4.8 – 5.7 GHz).

Characteristic mode analysis (CMA) has gradually been employed in the design and development of MTS-based CP antennas [17], [18], [19], [20]. In [17], an MTS-based CP patch antenna with cross-slot ground plane and sequentially-rotated feed network achieves an IBW of 28.2% (4.8 – 6.35 GHz) and 3-dB ARBW of 20.9% (6.8 – 9.7 GHz). In [18], a 2 × 2 clusters non-uniform MTS-based CP antenna array with Wilkinson power divider feed network achieves an IBW of 49.6% (6.05 – 10.04 GHz) and 3-dB ARBW of 33.13% (7 – 9.78 GHz). In [19], a 4 × 4 loop-shaped MTS-based CP antenna with circular ground plane achieves a fractional IBW and 3-dB ARBW of 14.7% (7.25 – 8.4 GHz). In [20], an MTS-based CP antenna with capacitive loading achieves an IBW of 22.85% (3.02 – 3.82 GHz) and 3-dB ARBW of 8.5% (3.33 – 3.63 GHz).

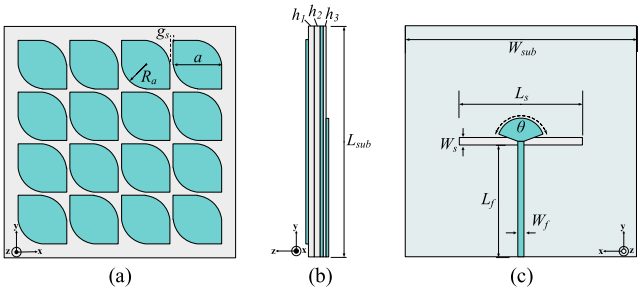

FIGURE 1. Geometry of one cluster of the leaf-shaped MTS-based CP stacked-patch antenna array: (a) front view, (b) side view, (c) rear view.

Specifically, this research proposes a quadruple-cluster leaf-shaped MTS-based CP stacked-patch antenna array with hybrid coupler feed network for sub-6 GHz 5G applications. The leaf-shaped MTS-based CP stacked-patch antenna is characterized by CMA. One cluster of the quadruple-cluster leaf-shaped MTS-based antenna array consists of 4 × 4 leaf-shaped MTS elements; and the hybrid coupler feed network is used to enhance IBW, ARBW, and antenna gain.

Simulations are carried out using CST Microwave Studio Suite and an antenna prototype is fabricated and experiment undertaken. The experiments are performed in an anechoic chamber and results compared with the simulations. The performance metrics include the impedance bandwidth ($|S_{11}| \leq -10$ dB), axial ratio bandwidth (AR $\leq$ 3 dB), antenna gain and radiation patterns.

II. ANTENNA DESIGN PROCESS

A. ONE CLUSTER OF THE LEAF-SHAPED MTS-BASED CP STACKED-PATCH ANTENNA ARRAY

Figures 1(a)-(c) show the geometry of one cluster of the leaf-shaped MTS-based CP stacked-patch antenna array. A single cluster of the leaf-shaped MTS-based CP stacked-patch antenna is realized by three stacks of FR-4 substrate: upper-, middle-, and lower-stacked substrates without air gap. The dimensions of the stacked substrates are 60 mm × 60 mm ($W_{sub} \times L_{sub}$) with a dielectric constant (ε_r) of 4.3. The thickness of the upper (h_1), middle (h_2), and lower substrates (h_3) are 1.6 mm, 1.6 mm, and 0.8 mm. The upper-stacked substrate contains 4 × 4 leaf-shaped MTS elements. The width and length of one leaf-shaped MTS element are identical (a = 12.6 mm), with a truncated curvature radius (R_a) of 6 mm. The gap between pairs of leaf-shaped MTS elements (g_s) is 0.8 mm. The rectangular-shaped slot on the middle-stack substrate functions as the ground plane. The dimensions of the rectangular-shaped slot ($W_s \times L_s$) are 2 mm × 32 mm. The lower-stacked substrate consists of a microstrip feed line

TABLE 1. Parameters and optimal dimensions of one cluster of the leaf-shaped MTS-based CP stacked-patch antenna array.

Parameters	W_{sub}	L_{sub}	h_1	h_2	h_3	a	R_a
Values (mm)	60	60	1.6	1.6	0.8	12.6	6
Parameters	g_s	W_s	L_s	W_f	L_f	θ	
Values (mm)	0.8	2	32	1.5	30	120°	

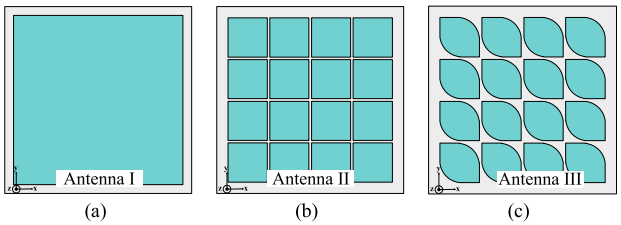

FIGURE 2. Evolutionary stages of the leaf-shaped MTS-based CP stacked-patch antenna: (a) Antenna I, (b) Antenna II, (c) Antenna III.

of 1.5 mm × 30 mm ($W_f \times L_f$) in dimension and a fan-shaped stub with a radius (θ) of 120°. The fan-shaped stub is used to improve impedance matching. Table 1 tabulates the parameters and optimal dimensions of one cluster of the leaf-shaped MTS-based CP stacked-patch antenna array.

In the design of CP MTS-based antennas, characteristic mode analysis (CMA) is utilized to characterize the surface current and radiating field on the perfect electric conductor structures [21]. In other words, the surface current and radiating field on the conducting structure determine the configuration and dimension of the CP MTS-based antennas [22]. The total current (J_{tot}) of the characteristic currents on the PEC structures can be calculated by equation (1) [23].

$$J_{tot} = \sum_{n=1}^{N} c_n J_n \tag{1}$$

where J_n is the characteristic current of mode n^{th} and c_n is the complex modal weighting coefficient of the n^{th} mode.

To realize circular polarization, the modal significance (MS) between two orthogonal modes must be identical, given MS $\geq$ 0.707. Meanwhile, the phase difference of characteristic angles (CA) is approximately ±90° [24] with orthogonal characteristic currents. The MS and CA can be calculated by equations (2) [25] and (3) [26], respectively.

$$\text{MS} = \left| \frac{1}{1 + j\lambda_n} \right| \tag{2}$$

$$\text{CA} = 180^\circ - \tan^{-1}(\lambda_n) \tag{3}$$

where MS and CA are the modal significance and characteristic angle of n^{th} mode, and λ_n is an eigenvalue.

Figures 2(a)-(c) show the three evolutionary stages of one cluster of the leaf-shaped MTS-based CP stacked-patch antenna array: first-generation (Antenna I), second-generation (Antenna II), and third-generation (Antenna III). In Antenna I, a square-shaped patch (54.4 mm × 54.4 mm) sits on lossless FR-4 substrate of 60 mm × 60 mm in dimension and 3.2 mm in thickness. In Antenna II, the

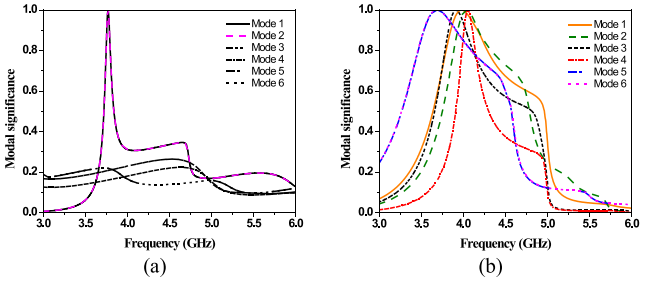

FIGURE 3. Simulated MS results of one cluster of the leaf-shaped MTS-based scheme: (a) Antenna I, (b) Antenna II.

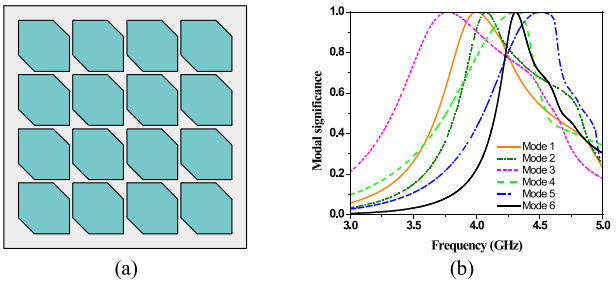

FIGURE 4. Corner-truncated square-shaped MTS-based scheme: (a) geometry, (b) MS.

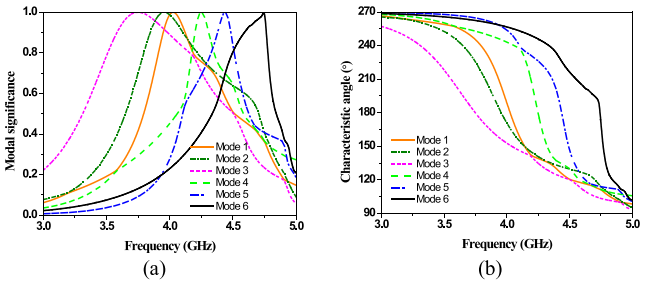

FIGURE 5. Simulated results of one cluster of the leaf-shaped MTS-based scheme of Antenna III: (a) MS, (b) CA.

square-shaped patch is uniformly segmented into 4 × 4 square-shaped MTS elements. The dimensions of one square-shaped MTS element are 12.6 mm × 12.6 mm, with the space between square-shaped MTS elements of 0.8 mm. In Antenna III, the square-shaped MTS elements are transmuted into the leaf-shaped MTS elements.

Figures 3(a)-(b) show the simulated MS of Antennas I and II, given MS $\geq$ 0.707. In Figure 3(a), the MS of Modes 1 and 2 of 1 are identical at 3.77 GHz, achieving the frequency resonance at 3.77 GHz. In Figure 3(b), the MS of Modes 5&6, 1&3, 1&2, and 2&4 of 1 are identical at 3.68 GHz, 3.94 GHz, 4 GHz, and 4.05 GHz, respectively, achieving the frequency resonance between 3.68 – 4.05 GHz.

Figure 4(a) shows the geometry of the corner-truncated square-shaped MTS-based scheme. In Figure 4(b), the simulated MS of Modes 1 – 6 are 1 at 4.01, 4.08, 3.78, 4.32, 4.51, and 4.31 GHz, achieving the frequency resonance between 3.78 – 4.51 GHz.

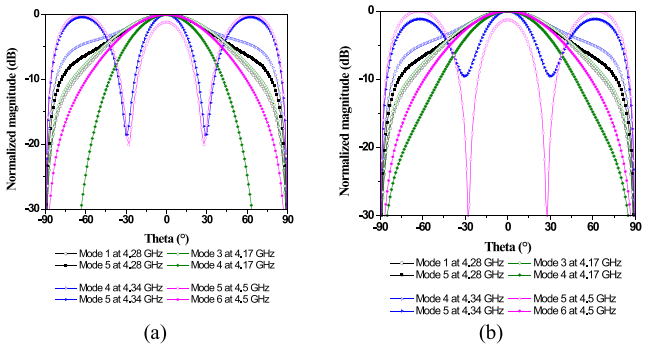

FIGURE 6. Modal 2D radiation patterns of Antenna III: (a) $\phi = 0°$, (b) $\phi = 90°$.

Figures 5(a)-(b) show the simulated CMA results Antenna III. In Figure 5(a), the MS of Modes 1 – 6 are 1 at 4.03, 3.95, 3.75, 4.25, 4.43, and 4.74 GHz, achieving the frequency resonance between 3.75 – 4.74 GHz. By comparison, one cluster of the leaf-shaped MTS-based scheme (Antenna III) achieved slightly wider frequency resonance (3.75 – 4.74 GHz), vis-a-vis the corner-truncated square-shaped MTS-based scheme (3.78 – 4.51 GHz).

To realize the CP radiation, the 4 × 4 square-shaped MTS elements (Antenna II) into the leaf-shaped MTS elements (Antenna III), given MS $\geq$ 0.707 and CA = $\pm 90°$). The MS of Modes 1&5, 3&4, 4&5, and 5&6 of 0.73, 0.79, 0.82, and 0.81 are identical at 4.28, 4.17, 4.34, and 4.5 GHz (Figure 5(a)), with the corresponding CA of 85°, 76°, 70°, and 72° (Figure 5(b)). The transformation of the square-shaped MTS elements (Antenna II) into the leaf-shaped MTS elements (Antenna III) enhances the frequency resonance, achieving the CP radiation between 4.17 – 4.5 GHz.

To validate the CP radiation, the amplitude and phase difference of 2D and 3D far-field radiation patterns of electric field of two orthogonal modes (Modes 1&5, 3&4, 4&5, and 5&6) in two planes ($\phi = 0°$ and $\phi = 90°$) must be identical and 90°, respectively. Figures 6(a)-(b) show the simulated results of normalized modal 2D radiation patterns of Antenna III in planes $\phi = 0°$ and $\phi = 90°$. The 2D radiation patterns of Modes 1&5, 3&4, 4&5, and 5&6 are of symmetrical broadside radiation patterns in planes $\phi = 0°$ and $\phi = 90°$.

The 3D radiation patterns of two orthogonal modes (Modes 1&5, 3&4, 4&5, and 5&6) are used to characterize the CP radiation in different orientations. Figures 7(a)-(d) respectively show the normalized modal 3D radiation patterns of Antenna III at 4.28 GHz, 4.17 GHz, 4.34 GHz, and 4.5 GHz, respectively. In Figure 6, the 3D radiation patterns of Modes 1&5, 3&4, and 5&6 are of symmetric-lobe radiation. The 2D and 3D radiation patterns of Modes 1&5, 3&4, and 5&6 demonstrate the CP radiation of Antenna III.

The CP radiation is further validated by the surface current distribution of Antenna III. The current distribution of two orthogonal modes (Modes 1&5, 3&4, and 5&6) must travel orthogonally along the edge of the leaf-shaped MTS elements. Figures 8(a)-(c) show the current distribution on one

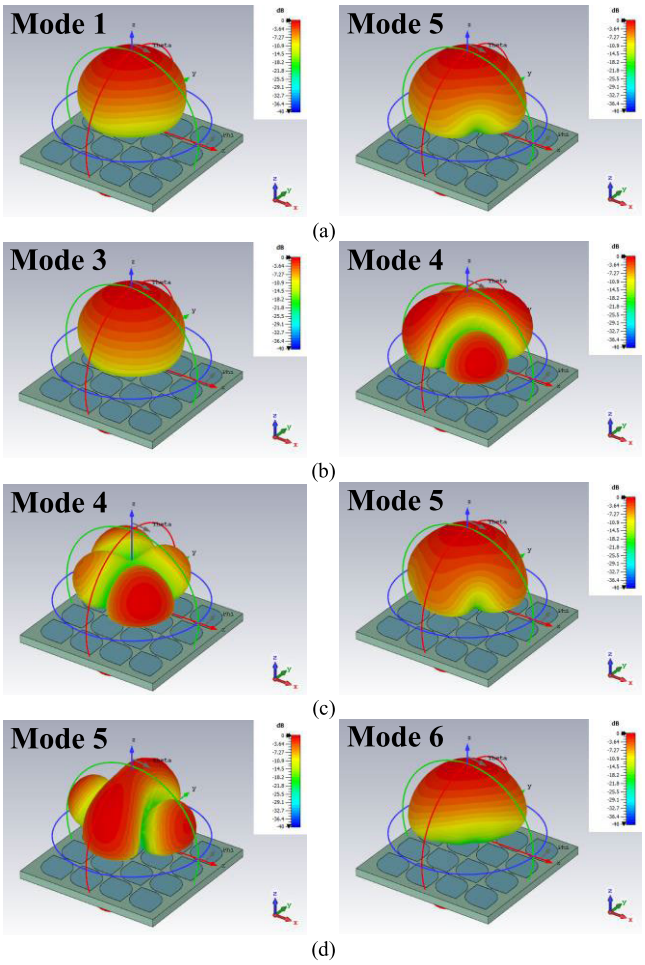

FIGURE 7. Modal 3D radiation patterns of Antenna III: (a) 4.28 GHz, (b) 4.17 GHz, (c) 4.34 GHz, (d) 4.5 GHz.

cluster of the leaf-shaped MTS elements (i.e., Antenna III) between orthogonal modes (Modes 1&5, 3&4, and 5&6) at 4.28, 4.17 GHz, and 4.5 GHz, respectively. In Figure 8(b), the surface current of Modes 3&4 at 4.17 GHz are non-orthogonal. Meanwhile, the surface current of Modes 1&5 at 4.28 GHz and Modes 5&6 at 4.5 GHz are orthogonal. The CP radiation of Antenna III is realized by two pairs of orthogonal current between Modes 1&5 and 5&6 at 4.28 and 4.5 GHz, respectively.

The CMA-based design process of one cluster of the leaf-shaped MTS-based CP stacked-patch antenna array is as follows:

i. Determining the dimension of one cluster of the leaf-shaped MTS-based CP stacked-patch antenna array based on the simulated MS results, given the frequency resonance of sub-6 GHz 5G spectrum. In Antenna I (square-shaped patch), the frequency resonance occurs once at 3.77 GHz (Modes 1 and 2), resulting in very narrow band frequency. In Antenna II, the square-shaped patch was transformed into 4 × 4 uniform square-shaped MTS elements to enhance the frequency

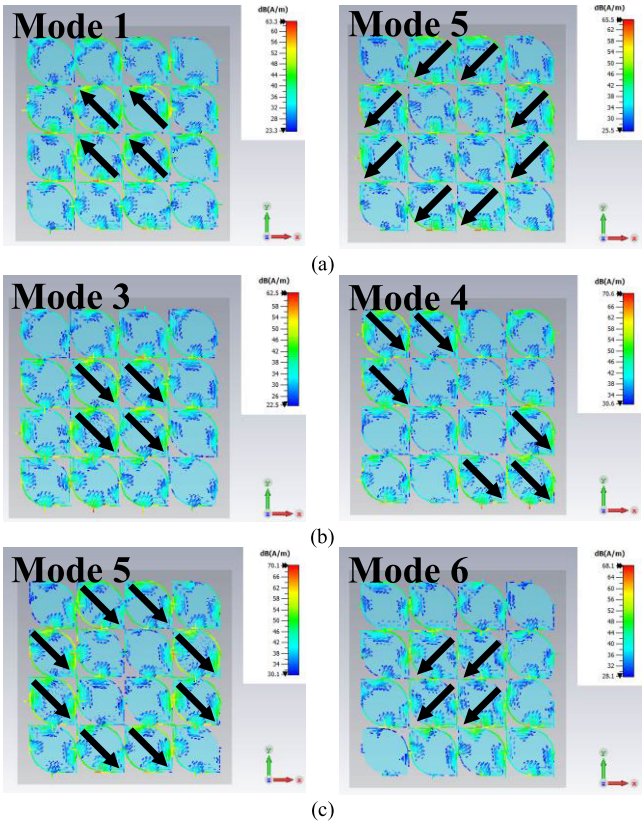

FIGURE 8. Surface current distributions of Antenna III: (a) 4.28 GHz, (b) 4.17 GHz, (c) 4.5 GHz.

resonance, achieving wider band frequency between 3.68 – 4.05 GHz (Modes 1 – 6).

ii. Transforming the 4 × 4 square-shaped MTS elements into the leaf-shaped MTS elements (Antenna III) to achieve CP radiation, with orthogonal Modes 1&5, 3&4, 4&5, and 5&6 (given MS ≥ 0.707 and CA = ±90°).

iii. To realize the CP radiation, the amplitude and phase difference of the electric-field components (i.e., 2D and 3D radiation patterns) of orthogonal Modes 1&5, 3&4, 4&5, and 5&6 must be identical and 90°, respectively. Thus, the normalized modal 2D radiation pattern is utilized to characterize the electric-field components of orthogonal Modes 1&5, 3&4, 4&5, and 5&6 in two planes ($\phi = 0°$ and $\phi = 90°$). Besides, the 3D radiation patterns of the electric-field components of orthogonal Modes 1&5, 3&4, and 5&6 must be of symmetric lobe in the +z direction.

iv. To verify the CP radiation of Antenna III, the surface current distribution of two orthogonal modes must travel in the orthogonal direction, as evidenced by Modes 1&5 and 5&6.

Figures 9(a)-(b) compare the simulated IBW, ARBW and gain of Antennas I, II, and III. In Figure 9(a), Antenna I exhibits an impedance mismatch ($|S_{11}| > -10$ dB), resulting in the absence of antenna gain (Figure 9(b)). Antenna II

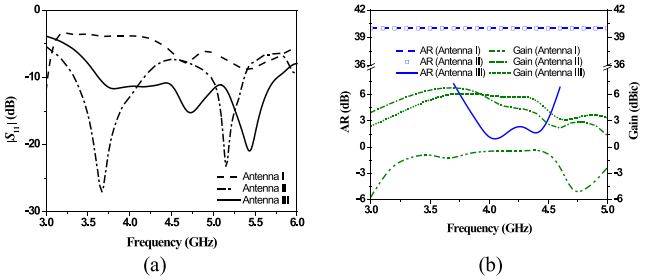

FIGURE 9. Simulated results of Antenna I, II, and III: (a) IBW, (b) ARBW and gain.

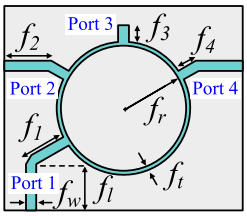

FIGURE 10. Geometry of the hybrid ring coupler.

achieves the first resonance between 3.34 – 4.17 GHz and the second resonance between 4.97 – 5.37 GHz. However, an impedance mismatch occurs between 4.17 – 4.9 GHz. The IBW of Antenna III at the center frequency (4 GHz) is 53.45% (3.62 – 5.76 GHz).

In Figure 9(b), the AR of Antennas I and II are greater than 3 dB (AR > 3 dB). In other words, the polarization of Antennas I and II are linear. The ARBW (AR ≤ 3 dB) at 4 GHz of Antenna III is 15.25% (3.89 – 4.5 GHz). Meanwhile, the maximum gain of Antennas II and III are 6.8 and 6.16 dBic at 3.7 and 3.8 GHz, respectively. The higher maximum antenna gain of Antenna II (6.8 dBic) could be attributed to better impedance matching at 3.7 GHz of Antenna II (-25.16 dB), vis-à-vis Antenna III (-11 dB).

B. HYBRID COUPLER FEED NETWORK DESIGN

Figure 10 shows the geometry of a hybrid ring coupler (i.e., rat-race coupler) [27]. The conventional hybrid ring coupler consists of a circular ring and a four-port microstrip line, which sit on FR-4 substrate. The four ports of the hybrid ring coupler include one input port (Port 1), one isolated port (Port 3), and two output ports (Ports 2 and 4). The hybrid ring coupler is used to divide power delivery with 180° phase difference between two output ports (Ports 2 and 4).

Figure 11(a) shows the magnitude $|S_{ij}|$ of the input port (Port 1) and the output ports 2 and 4 ($|S_{21}|$ and ($|S_{41}|$). Figure 11(b) depicts the phase difference of $|S_{21}|$ and $|S_{41}|$. In Figure 11(a), $|S_{11}|$ of Port 1 is below -18 dB between 3.5 – 4.5 GHz, while $|S_{21}|$ and $|S_{41}|$ of Ports 2 and 4 are between -3 dB and -4 dB between 3.5 – 4.5 GHz. In Figure 11(b), the phase difference between Ports 2 and 4 is approximately 180° between 3.5 – 4.5 GHz. The optimal dimensions of the hybrid ring coupler at the center frequency of 4 GHz are as follows:

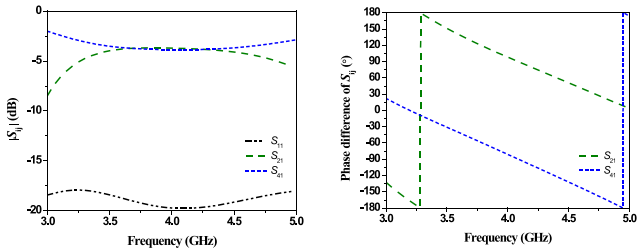

FIGURE 11. Simulated results of the hybrid ring coupler: (a) $|S_{ij}|$, (b) phase difference of S_{ij}.

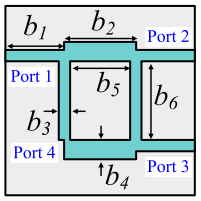

FIGURE 12. Geometry of the quadrature hybrid coupler.

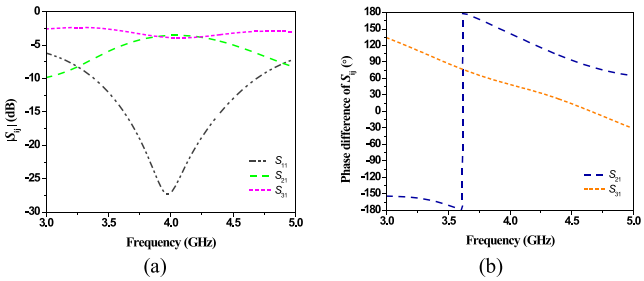

FIGURE 13. Simulated results of the quadrature hybrid coupler: (a) $|S_{ij}|$, (b) phase difference of S_{ij}.

$f_w = 1.5$ mm, $f_l = 7.5$ mm, $f_r = 9.75$ mm, $f_t = 0.65$ mm, $f_1 = 7$ mm, $f_2 = 7.7$ mm, $f_3 = 3$ mm, and $f_4 = 3.5$ mm.

Figure 12 shows the geometry of a quadrature hybrid coupler (i.e., branch-line coupler) [28]. The conventional quadrature hybrid coupler consists of two series arms, two shunt arms, and two microstrip lines. The proposed quadrature hybrid coupler comprises four ports: one input port (Port 1), one isolated port (Port 4), and two output ports (Ports 2 and 3). The quadrature hybrid coupler is utilized to divide power delivery with 90° phase difference between two output ports (Ports 2 and 3).

Figure 13(a) shows the magnitude $|S_{ij}|$ of the input port (Port 1) and the output ports 2 and 3 ($|S_{21}|$ and ($|S_{31}|$) and Figure 13(b) depicts the phase difference of S_{21} and S_{31}. In Figure 13(a), $|S_{11}|$ of Port 1 is below -10 dB between 3.38 – 4.68 GHz, while $|S_{21}|$ and $|S_{31}|$ are between -3 dB and -5 dB between 3.65 – 4.5 GHz. In Figure 13(b), the phase difference between Ports 2 and 3 is approximately 90° between 3.61 – 4.5 GHz. The optimal dimensions of the quadrature hybrid coupler at the center frequency of 4 GHz

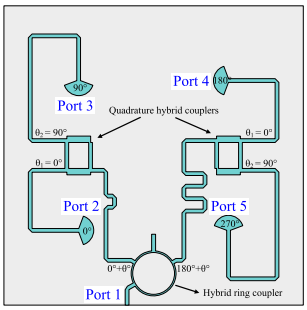

FIGURE 14. Geometry of the proposed hybrid coupler feed network.

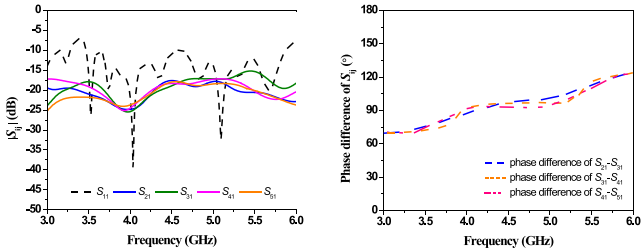

FIGURE 15. Simulated results of the proposed hybrid coupler feed network: (a) $|S_{ij}|$, (b) phase difference of S_{ij}.

are as follows: $b_1 = 7.75$ mm, $b_2 = 9.5$ mm, $b_3 = 1.5$ mm, $b_4 = 2.6$ mm, $b_5 = 8$ mm, and $b_6 = 10.4$ mm.

Figure 14 shows the geometry of the proposed hybrid coupler feed network. The proposed hybrid coupler feed network consists of a hybrid ring coupler and a two-element quadrature hybrid coupler. The hybrid ring coupler is connected to the two-element quadrature hybrid coupler to function as a hybrid coupler feed network. The proposed hybrid coupler feed network includes one input port (Port I) and four output ports (Ports II, III, IV, and V). The output ports are sequentially perpendicular to one another. The proposed hybrid coupler feed network could achieve phase quadrature with equal magnitude for CP radiation.

Figures 15(a)-(b) show the magnitude $|S_{11}|$ of the input port (Port 1) and $|S_{21}|$, $|S_{31}|$, $|S_{41}|$, and $|S_{51}|$ of the output ports (Ports 2, 3, 4, and 5) and the phase difference between output ports. In Figure 15(a), $|S_{11}|$ of the input port is below -10 dB between 3.4 – 5.9 GHz, while those of the output ports are between -17.5 dB and -25.5 dB between 3.6 – 5.25 GHz. In Figure 15(b), the phase difference between output ports are approximately 90° between 3.7 – 5 GHz.

C. THE PROPOSED QUADRUPLE-CLUSTER LEAF-SHAPED MTS-BASED CP STACKED-PATCH ANTENNA ARRAY WITH HYBRID COUPLER FEED NETWORK

Figures 16(a)-(c) show the geometry of the proposed CMA-based quadruple-cluster leaf-shaped MTS-based CP stacked-patch antenna array with hybrid coupler feed network. The proposed quadruple-cluster leaf-shaped MTS-based antenna array scheme is realized using three stacks of FR-4 substrate

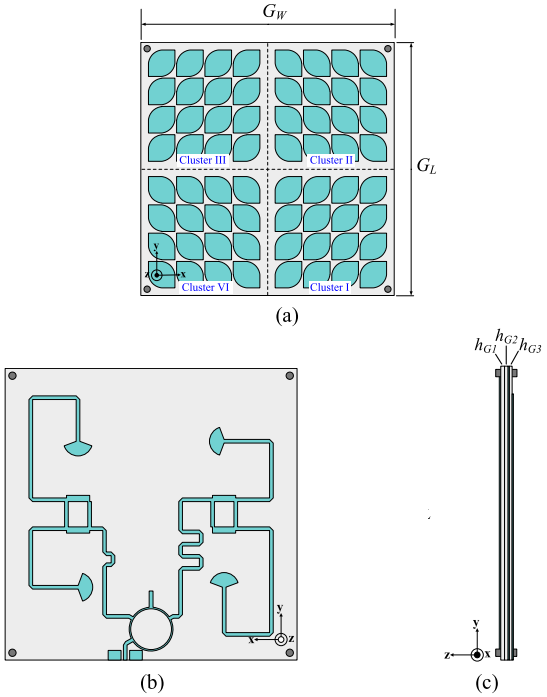

FIGURE 16. Geometry of the proposed CMA-based quadruple-cluster leaf-shaped MTS-based CP stacked-patch antenna array with hybrid coupler feed network: (a) front view, (b) rear view (reverse side), (c) side view.

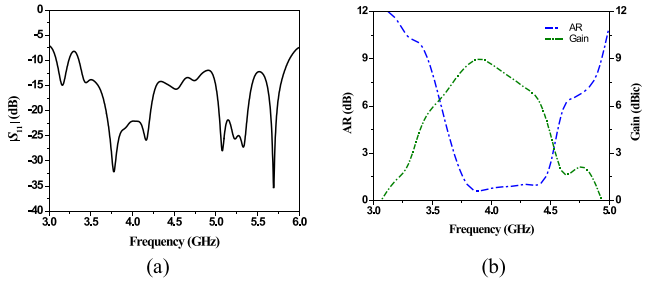

FIGURE 17. Simulated results of the proposed CMA-based quadruple-cluster leaf-shaped MTS-based CP stacked-patch antenna array with hybrid coupler feed network: (a) IBW, (b) ARBW and gain.

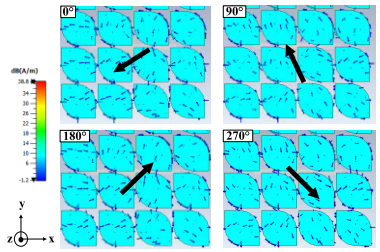

FIGURE 18. Surface current distribution at 4 GHz of the proposed CMA-based quadruple-cluster leaf-shaped MTS-based CP stacked-patch antenna array with hybrid coupler feed network.

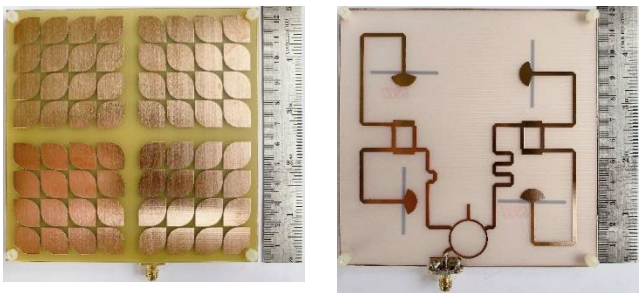

FIGURE 19. Antenna prototype of the proposed CMA-based quadruple-cluster leaf-shaped MTS-based CP stacked-patch antenna array with hybrid coupler feed network: (a) front view, (b) rear view.

without airgap: upper, middle and lower-stacked substrates. The dimensions of the proposed quadruple-cluster antenna array scheme are 120 mm × 120 mm ($G_W \times G_L$), and the thickness of the upper (h_{G1}), middle (h_{G2}), and lower-stacked (h_{G3}) substrates are 1.6 mm, 1.6 mm, and 0.8 mm. The proposed CMA-based quadruple-cluster leaf-shaped MTS-based CP stacked-patch antenna array consists of four clusters of 4 × 4 leaf-shaped MTS-based elements: Clusters I, II, III, and IV.

Figures 17(a)-(b) show the simulated IBW ($|S_{11}| \leq$ -10 dB), ARBW (AR $\leq$ 3 dB), and gain of the proposed CMA-based quadruple-cluster leaf-shaped MTS-based CP stacked-patch antenna array with hybrid coupler feed network. In Figure 17(a), the simulated IBW is 63% (3.35 – 5.87 GHz) at the center frequency of 4 GHz. In Figure 17(b), the simulated ARBW at 4 GHz is 21.25 % (3.68 – 4.53 GHz) with a maximum gain of 9.1 dBic at 3.9 GHz.

Figures 18(a)-(b) respectively show the surface current distribution at the center frequency of 4 GHz corresponding to phases 0°, 90°, 180°, and 270° of the proposed quadruple-cluster leaf-shaped antenna array with hybrid coupler feed network. The electric field vectors on the leaf-shaped MTS elements travel clockwise in the +z direction, resulting in right-handed circular polarization (RHCP).

III. EXPERIMENTAL RESULTS

Figures 19(a)-(b) show the front and rear of a prototype of the proposed CMA-based quadruple-cluster leaf-shaped MTS-based CP stacked-patch antenna array with hybrid coupler feed network. Figure 20 shows the experimental setup in an anechoic chamber. The experiments were carried out using a vector network analyzer (Rohde&Schwarz ZNLE6 model). A pair of Conical Log Spiral antennas (ETS-Lindgren Model 3102 Series) are used as transmitting antennas. The antennas are used to verify RHCP and LHCP radiations of the antenna prototype (i.e., the receiving antenna). The far-field distance [29] between the transmitting and receiving antennas is 4 m.

The AR of the antenna prototype is measured by the co-polarization (co-pol) and cross-polarization (cross-pol) of electric fields. The co-pol and cross-pol electric fields between the transmitting and receiving antennas correspond to $|E_{co-pol}|$ and $|E_{cross-pol}|$, which in turn correspond to

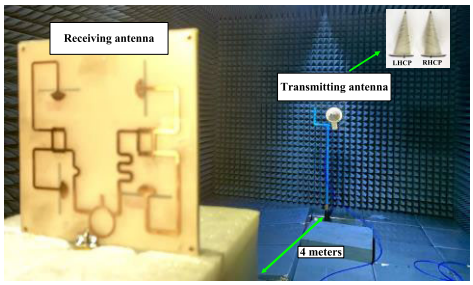

FIGURE 20. Experimental setup of the proposed CMA-based quadruple-cluster leaf-shaped MTS-based CP stacked-patch antenna array with hybrid coupler feed network.

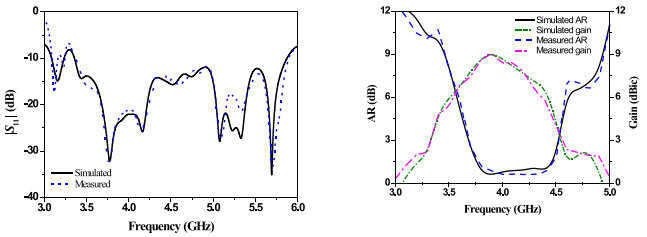

(a) (b)

FIGURE 21. Simulated and measured results of the proposed CMA-based quadruple-cluster leaf-shaped MTS-based CP stacked-patch antenna array with hybrid coupler feed network: (a) IBW, (b) ARBW and gain.

RHCP and LHCP. The AR is determined by equation (4) [30].

$$AR(\text{dB}) = 20\log\left(\frac{|E_{co-pol}| + |E_{cross-pol}|}{|E_{co-pol}| - |E_{cross-pol}|}\right) \quad (4)$$

where $|E_{co-pol}|$ and $|E_{cross-pol}|$ are the electric field magnitudes of the co- and cross-pol between the transmitting and receiving antennas.

Figures 21(a)-(b) compare the simulated and measured IBW, ARBW and gain of the proposed CMA-based quadruple-cluster leaf-shaped MTS-based CP stacked-patch antenna array with hybrid coupler feed network. The simulated IBW ($|S_{11}| \leq -10$ dB) and ARBW (AR ≤ 3 dB) are 63% (3.35 – 5.87 GHz) and 21.25 % (3.68 – 4.53 GHz), with the maximum gain of 9.1 dBic at 3.9 GHz. Meanwhile, the measured IBW and ARBW are 62.5% (3.4 – 5.9 GHz) and 21% (3.8 – 4.54 GHz), with the maximum gain of 9.04 dBic at 3.9 GHz. The simulated and measured results are agreeable.

Figures 22(a)-(c) show the simulated and measured RHCP and LHCP radiation patterns in the xy- and yz-planes of the proposed quadruple-cluster leaf-shaped antenna array with hybrid coupler feed network at 3.8 GHz, 4 GHz, and 4.5 GHz, respectively. The simulated and measured RHCP and LHCP are reasonably agreeable despite some discrepancies. Specifically, the discrepancy between the simulated and measured radiation patterns could be attributed to fabrication challenges and errors, including antenna rotational mounts, coaxial cable attenuation [31].

Meanwhile, the high sidelobe level could be attributed to the leaf-shaped MTS elements (to convert linear to circular

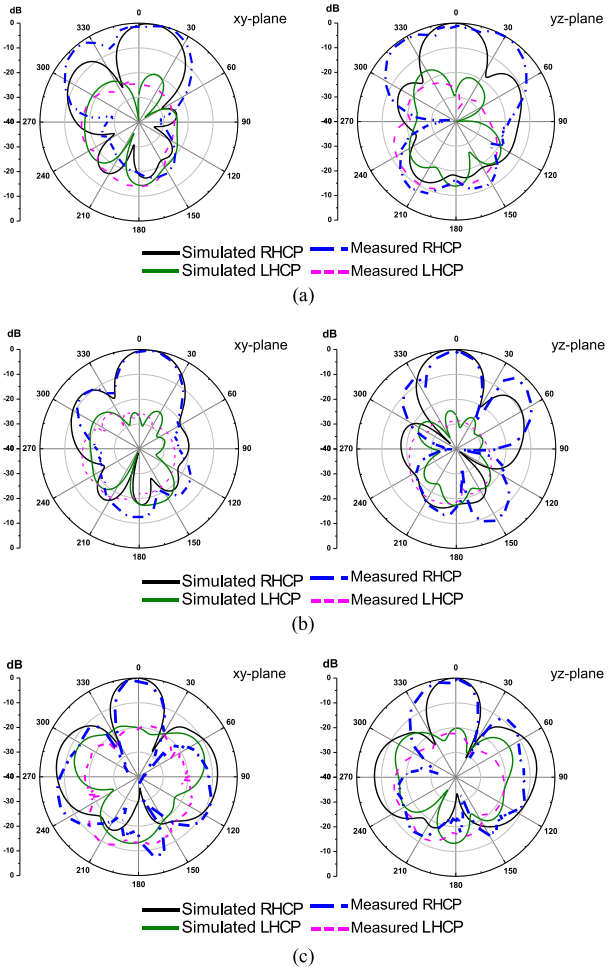

(a)

(b)

(c)

FIGURE 22. Simulated and measured RHCP and LHCP radiation patterns at: (a) 3.8 GHz, (b) 4 GHz, (c) 4.5 GHz.

polarization); and to the four-cluster MTS-based antenna array (to enhance the bandwidth and gain) [32]. As a result, the Dolph-Chebyshev method [33], Taylor method [34], and several other techniques [35], [36], [37] have been adopted to suppress the high side lobe level.

Table 2 compares the existing CP antennas for 5G spectra and the proposed CMA-based quadruple-cluster leaf-shaped MTS-based CP stacked-patch antenna array with hybrid coupler feed network in terms of antenna type, operating frequency bands, IBW, ARBW, maximum gain, and electrical dimension.

In [17], a low-complexity square-shaped MTS-based CP antenna with meandering microstrip line and cross-slot ground plane suffers from narrow IBW. In [19], a rectangular-ring MTS-based CP antenna with slanted-slot ground plane suffers from very narrow IBW and ARBW despite straightforward structure. In [21], an H-shaped MTS-based CP antenna suffers from narrow ARBW and bulkiness. In [24], a non-uniform MTS-based CP antenna suffers from very narrow IBW and ARBW apart from high-complexity feed structure.

TABLE 2. Comparison between existing MTS-based CP antennas and the proposed CMA-based quadruple-cluster leaf-shaped MTS-based CP stacked-patch antenna array with hybrid coupler feed network.

Ref.	f_c (GHz)	IBW (%)	ARBW (%)	Max. gain (dBic)	Antenna structure and application	Analysis technique	Electrical dimension at λ_L^3
[17]	5.5	28.2	20.9	9.7	• Type: rectangular-shaped MTS-based stacked-patch antenna • No. of substrate layers: two layers without air gap • Upper and lower substrates: F4B, $\varepsilon_r = 3.5$, $\tan\delta = 0.003$ • Feeding technique: microstrip meander-line • Application: C-band communications	Modal analysis method	1.00×1.00×0.070
[19]	7.82	14.7	14.7	8.6	• Type: rectangular-ring MTS-based stacked-patch antenna • No. of substrate layers: two layers with air gap • Upper and lower substrates: Fr-4, $\varepsilon_r = 4.2$, $\tan\delta = 0.02$ • Feeding technique: microstrip meander-line • Application: X-band communications	Modal analysis method	1.30×1.30×0.137
[21]	5	8.8	14.3	8.5	• Type: H-shaped MTS-based stacked-patch antenna • No. of substrate layers: two layers without air gap • Upper and lower substrates: Rogers 4003C, $\varepsilon_r = 3.38$, $\tan\delta = 0.0027$ • Feeding technique: microstrip line • Application: C-band communications	Modal analysis method	1.45×1.45×0.074
[24]	2.15	13.9	17.43	8	• Type: non-uniform MTS-based stacked-patch antenna • No. of substrate layers: four layers without air gap • 1st substrate: Rogers TMM3, $\varepsilon_r = 3.46$, $\tan\delta = 0.002$ 2nd and 4th substrates: Rogers TMM4, $\varepsilon_r = 4.7$, $\tan\delta = 0.002$ 3rd substrate: Rogers 4450B, $\varepsilon_r = 3.3$, $\tan\delta = 0.004$ • Feeding technique: microstrip line with coaxial probe • Application: S-band nanosatellite technology	Modal analysis method	0.71×0.71×0.068
[38]	2.45	69.4	46.5	12.8	• Type: rectangular-ring with diagonal MTS-based stacked-patch cavity antenna array • No. of substrate layers: three layers with air gap • Upper and middle substrates: Fr-4, $\varepsilon_r = 4.2$, $\tan\delta = 0.02$ Lower substrate: Rogers 4350B, $\varepsilon_r = 3.66$, $\tan\delta = 0.0031$ • Feeding technique: microstrip-line feed network • Application: WI-FI	Full-wave method	1.63×1.63×0.070
[39]	2.15	52.5	31.3	7.01	• Type: rectangular-shaped MTS-based stacked-patch antenna • No. of substrate layers: two layers without air gap • Upper substrate: F4B, $\varepsilon_r = 3.5$, $\tan\delta = 0.0027$ lower substrate: Fr-4, $\varepsilon_r = 4.4$, $\tan\delta = 0.02$ • Feeding technique: dual-port microstrip line • Application: Wireless communications	Modal analysis method	0.71×0.71×0.040
[40]	27.5	34.7	20.1	11	• Type: rectangular-ring MTS-based stacked-patch antenna • No. of substrate layers: two layers without air gap • Upper and lower substrates: Rogers 5880, $\varepsilon_r = 2.2$, $\tan\delta = 0.0009$ • Feeding technique: corner-truncated rectangular-shaped patch with a coaxial probe • Application: 5G millimeter-wave systems	Full-wave method	1.10×1.10×0.093
[41]	5.4	29.11	9.02	6.34	• Type: slanted rectangular-shaped MTS-based stacked-patch antenna • No. of substrate layers: two layers without air gap • Upper and lower substrates: Rogers 4003, $\varepsilon_r = 3.38$, $\tan\delta = 0.0027$ • Feeding technique: microstrip line • Application: C-band radar and satellite communications	Modal analysis method	0.52×0.52×0.078
[42]	6.15	62.7	56.7	14.1	• Type: mushroom-type MTS-based stacked-patch antenna array • No. of substrate layers: two layers without air gap • Upper substrate: Duroid, $\varepsilon_r = 2.65$, $\tan\delta = 0.0027$ lower substrate: F4B, $\varepsilon_r = 2.2$, $\tan\delta = 0.0009$ • Feeding technique: sequential-phase feed network • Application: C-band communications	Full-wave method	1.64×1.64×0.072

TABLE 2. *(Continued.)* **Comparison between existing MTS-based CP antennas and the proposed CMA-based quadruple-cluster leaf-shaped MTS-based CP stacked-patch antenna array with hybrid coupler feed network.**

Ref.	f_c (GHz)	IBW (%)	ARBW (%)	Max. gain (dBic)	Antenna structure and application	Analysis technique	Electrical dimension at λ_L^3
[43]	6	117	105.7	12.5	• Type: ellipse-shaped with rectangular-ring MTS-based stacked-patch antenna array • No. of substrate layers: two layers without air gap • Upper substrate: F4BM, $\varepsilon_r = 2.2$, $\tan\delta = 0.004$ lower substrate: Rogers 4003, $\varepsilon_r = 3.55$, $\tan\delta = 0.0027$ • Feeding technique: sequentially-rotated feed network with resistors • Application: UWB communications	Full-wave method	0.60×0.60×0.030
[44]	5.5	39.25	17.77	7	• Type: multi-shaped MTS-based stacked-patch antenna • No. of substrate layers: two layers without air gap • Upper and lower substrates: Fr-4, $\varepsilon_r = 4.4$, $\tan\delta = 0.02$ • Feeding technique: microstrip line • Application: C-band satellite communications	Full-wave method	0.65×0.65×0.060
[45]	5	38.6	32	11.18	• Type: corner-truncated rectangular-shaped MTS-based stacked-patch antenna array • No. of substrate layers: two layers with air gap • Upper substrate: Fr-4, $\varepsilon_r = 4.4$, $\tan\delta = 0.02$ lower substrate: Rogers 5880, $\varepsilon_r = 4.4$, $\tan\delta = 0.0009$ • Feeding technique: dual-port sequential-phase feed network • Application: C-band communications	Full-wave method	1.40×1.40×0.069
[46]	5.5	41.45	23.16	13.5	• Type: square-shaped MTS-based stacked-patch antenna array • No. of substrate layers: two layers without air gap • Upper and lower substrates: Rogers 4003, $\varepsilon_r = 3.38$, $\tan\delta = 0.0027$ • Feeding technique: sequentially-rotated feed network with coaxial probe • Application: Wireless communications	Full-wave method	1.60×1.60×0.065
[47]	5.9	42.1	30	7.6	• Type: non-uniform MTS-based stacked-patch antenna • No. of substrate layers: two layers without air gap • Upper and lower substrates: F4B, $\varepsilon_r = 3.5$, $\tan\delta = 0.0018$ • Feeding technique: corner-truncated patch with coaxial probe • Application: C-band communications	Full-wave method	0.80×0.80×0.060
[48]	1.7	15.7	13	9	• Type: asymmetric MTS-based stacked-patch antenna • No. of substrate layers: three layers without air gap • Upper and lower substrates: Rogers 4003C, $\varepsilon_r = 3.4$, $\tan\delta = 0.0027$ • Middle substrate: Expanded polystyrene foam • Feeding technique: rectangular-shaped patch with a coaxial probe • Application: L-band satellite systems	Full-wave method	0.67×0.64×0.120
[49]	9.6	41.45	23.16	13.5	• Type: corner-truncated square-shaped MTS-based stacked-patch antenna array • No. of substrate layers: two layers without air gap • Upper and lower substrates: Rogers 4003, $\varepsilon_r = 3.38$, $\tan\delta = 0.0027$ • Feeding technique: sequentially-rotated feed network • Application: X-band communications	Full-wave method	1.60×1.60×0.065
[50]	5.5	45.6	23.4	7.6	• Type: rectangular-shaped MTS-based stacked-patch antenna • No. of substrate layers: two layers without air gap • Upper and lower substrates: Rogers 4003, $\varepsilon_r = 3.38$, $\tan\delta = 0.0027$ • Feeding technique: corner-truncated patch • Application: C-band communications	Full-wave method	0.58×0.58×0.056
This work	**4**	**62.5**	**21**	**9.04**	**• Type: leaf-shaped MTS-based stacked-patch antenna array** **• No. of substrate layers: three layers without air gap** **• Upper, middle and lower substrates: Fr-4, $\varepsilon_r = 4.3$, $\tan\delta = 0.025$** **• Feeding technique: hybrid coupler feed network** **• Application: Sub-6 GHz 5G communications**	**Modal analysis method**	**1.30×1.30×0.040**

f_c is the center frequency of the CP antennas for 5G spectra; and λ_L is the free-space wavelength corresponding to the lowest operating frequency.

In [38], a rectangular ring with diagonal MTS-based CP cavity antenna array achieves wide IBW, ARBW, and high gain; but suffers from high-complexity feed network structure and bulkiness. In [39], a rectangular-shaped MTS-based CP antenna with circular-ring slot ground plane and dual-port microstrip line feed suffers from low gain despite wide IBW. In [40], a low-complexity rectangular-ring MTS-based CP antenna suffers from narrow IBW. In [41], a slanted rectangular-shaped MTS-based suffers from very narrow IBW and ARBW.

In [42], a mushroom-type MTS-based CP antenna array achieves wide IBW, ARBW and high gain; but it suffers from bulkiness and fabrication challenges. In [43], an ellipse-shaped with rectangular-ring MTS-based CP antenna suffers from high complexity despite wide IBW, ARBW, and high gain. In addition, its sequentially-rotated feed network requires multiple resistors, making the feed network very complex. In [44], a multi-shaped MTS-based CP antenna suffers from narrow ARBW and low gain.

In [45], a corner-truncated rectangular-shaped MTS-based CP antenna array suffers from narrow IBW and bulkiness despite wide ARBW. In [46], a square-shaped MTS-based CP antenna array suffers from narrow IBW and bulkiness. In [47], a non-uniform MTS-based CP antenna achieves wide ARBW but low gain. In [48], a low-profile asymmetric MTS-based CP antenna suffers from narrow IBW and ARBW. In comparison, the proposed CMA-based quadruple-cluster leaf-shaped MTS-based CP stacked-patch antenna array achieves wide IBW of 62.5% (3.4 – 5.9 GHz) and ARBW of 21% (3.8 – 4.54 GHz), with low-complexity structure. In [49], a four-cluster corner-truncated square-shaped MTS-based CP antenna array with sequentially-rotated feed network achieved high gain but suffers from narrow IBW and bulkiness. Unlike in [49] which characterized the circular polarization of the corner-truncated square-shaped MTS-based CP antenna array by using the full-wave method, this research uses CMA to characterize the circular polarization of the leaf-shaped MTS-based CP stacked-patch antenna. In [50], a 4 × 4 square-shaped MTS-based CP patch antenna was used to enhance the CP bandwidth of the single-fed CP patch antenna. However, the proposed scheme achieved narrow IBW and low gain.

IV. CONCLUSION

This research proposes a quadruple-cluster leaf-shaped MTS-based CP stacked-patch antenna array with hybrid coupler feed network for sub-6 GHz 5G communication. One cluster of the quadruple-cluster leaf-shaped MTS-based antenna array consists of 4 × 4 leaf-shaped MTS elements. In the study, the leaf-shaped MTS-based antenna is characterized by CMA. The CMA results demonstrate that the surface current distribution on the 4 × 4 leaf-shaped MTS elements of Modes 1&5 and 5&6 at 4.28 and 4.5 GHz are orthogonal. Specifically, the hybrid coupler feed network is used to enhance IBW, ARBW, and gain. Simulations are performed and an antenna prototype is fabricated and experiments carried out. The simulated IBW and ARBW at the center frequency (4 GHz) are 63% (3.35 – 5.87 GHz) and 21.25 % (3.68 – 4.53 GHz), with a maximum gain of 9.1 dBic at 3.9 GHz. The measured IBW, ARBW, and maximum gain are 62.5% (3.4 – 5.9 GHz), 21% (3.8 – 4.54 GHz), and 9.04 dBic at 3.9 GHz. Besides, the simulated and measured RHCP and LHCP radiation patterns are in good agreement. Essentially, the proposed quadruple-cluster leaf-shaped MTS-based CP stacked-patch antenna array scheme is operationally suitable for sub-6 GHz 5G applications.

REFERENCES

[1] C.-X. Wang, F. Haider, X. Gao, Y. Yang, D. Yuan, H. M. Aggoune, H. Haas, S. Flectcher, and E. Hepsaydir, "Cellular architecture and key technologies for 5G wireless communication networks," *IEEE Commun. Mag.*, vol. 52, no. 2, pp. 122–130, Feb. 2014.

[2] S. Kumar, A. S. Dixit, R. R. Malekar, H. D. Raut, and L. K. Shevada, "Fifth generation antennas: A comprehensive review of design and performance enhancement techniques," *IEEE Access*, vol. 8, pp. 163568–163593, 2020.

[3] H. T. Chattha, M. K. Ishfaq, B. A. Khawaja, A. Sharif, and N. Sheriff, "Compact multiport MIMO antenna system for 5G IoT and cellular handheld applications," *IEEE Antennas Wireless Propag. Lett.*, vol. 20, no. 11, pp. 2136–2140, Nov. 2021.

[4] J.-H. Han and N.-H. Myung, "Novel feed network for circular polarization antenna diversity," *IEEE Antennas Wireless Propag. Lett.*, vol. 13, pp. 979–982, 2014.

[5] U. Ullah, M. Al-Hasan, S. Koziel, and I. B. Mabrouk, "A series inclined slot-fed circularly polarized antenna for 5G 28 GHz applications," *IEEE Antennas Wireless Propag. Lett.*, vol. 20, no. 3, pp. 351–355, Mar. 2021.

[6] K. X. Wang and H. Wong, "A circularly polarized antenna by using rotated-stair dielectric resonator," *IEEE Antennas Wireless Propag. Lett.*, vol. 14, pp. 787–790, 2015.

[7] C. Zhu, G. Xu, D. Ding, J. Wu, W. Wang, Z.-X. Huang, and X.-L. Wu, "Low-profile wideband millimeter-wave circularly polarized antenna with hexagonal parasitic patches," *IEEE Antennas Wireless Propag. Lett.*, vol. 20, no. 9, pp. 1651–1655, Sep. 2021.

[8] L. Ge, X. Yang, M. Li, and H. Wong, "Polarization-reconfigurable magnetoelectric dipole antenna for 5G Wi-Fi," *IEEE Antennas Wireless Propag. Lett.*, vol. 16, pp. 1504–1507, 2017.

[9] Q. W. Lin, H. Wong, X. Y. Zhang, and H. W. Lai, "Printed meandering probe-fed circularly polarized patch antenna with wide bandwidth," *IEEE Antennas Wireless Propag. Lett.*, vol. 13, pp. 654–657, 2014.

[10] A. Dadgarpour, M. Sharifi Sorkherizi, and A. A. Kishk, "High-efficient circularly polarized magnetoelectric dipole antenna for 5G applications using dual-polarized split-ring resonator lens," *IEEE Trans. Antennas Propag.*, vol. 65, no. 8, pp. 4263–4267, Aug. 2017.

[11] A. Kumar, A. A. Althuwayb, D. Chaturvedi, R. Kumar, and F. Ahmadfard, "Compact planar magneto-electric dipole-like circularly polarized antenna," *IET Commun.*, vol. 16, no. 20, pp. 2448–2453, Sep. 2022.

[12] M. Saravanakumar, A. Kumar, and S. Raghawan, "Substrate integrated waveguide fed wideband circularly polarised antenna with parasitic patches," *Defence Sci. J.*, vol. 69, no. 1, pp. 87–92, Jan. 2019.

[13] N. Supreeyatitikul, T. Lertwiriyaprapa, and C. Phongcharoenpanich, "S-shaped metasurface-based wideband circularly polarized patch antenna for C-band applications," *IEEE Access*, vol. 9, pp. 23944–23955, 2021.

[14] N. Supreeyatitikul, D. Torrungrueng, and C. Phongcharoenpanich, "Quadri-cluster broadband circularly-polarized sequentially-rotated metasurface-based antenna array for C-band satellite communications," *IEEE Access*, vol. 9, pp. 67015–67027, 2021.

[15] N. Supreeyatitikul, A. Boonpoonga, and C. Phongcharoenpanich, "Z-shaped metasurface-based wideband circularly polarized Fabry–Pérot antenna for C-band satellite technology," *IEEE Access*, vol. 10, pp. 59428–59441, 2022.

[16] N. Supreeyatitikul, P. Akkaraekthalin, and C. Phongcharoenpanich, "Single-layer wideband CP CPW-fed antenna based on staircase-shape metasurface," in *Proc. Int. Symp. Antennas Propag. (ISAP)*, Taiwan, Oct. 2021, pp. 1–2.

[17] X. Gao, G. Tian, Z. Shou, and S. Li, "A low-profile broadband circularly polarized patch antenna based on characteristic mode analysis," *IEEE Antennas Wireless Propag. Lett.*, vol. 20, no. 2, pp. 214–218, Feb. 2021.

[18] X. Gao, S. Yin, G. Wang, C. Xue, and X. Xie, "Broadband low-RCS circularly polarized antenna realized by nonuniform metasurface," *IEEE Antennas Wireless Propag. Lett.*, vol. 21, no. 12, pp. 2417–2421, Dec. 2022.

[19] S. Genovesi and F. A. Dicandia, "Characteristic modes analysis of a near-field polarization-conversion metasurface for the design of a wideband circularly polarized X-band antenna," *IEEE Access*, vol. 10, pp. 88932–88940, 2022.

[20] Y. Juan, W. Yang, and W. Che, "Miniaturized low-profile circularly polarized metasurface antenna using capacitive loading," *IEEE Trans. Antennas Propag.*, vol. 67, no. 5, pp. 3527–3532, May 2019.

[21] C. Zhao and C. F. Wang, "Characteristic mode design of wide band circularly polarized patch antenna consisting of H-shaped unit cells," *IEEE Access*, vol. 6, pp. 25292–25299, 2018.

[22] R. F. Harrington and J. R. Mautz, "Theory of characteristic modes for conducting bodies," *IEEE Trans. Antennas Propag.*, vol. AP-19, no. 5, pp. 622–628, Sep. 1971.

[23] M. Khan and D. Chatterjee, "Characteristic mode analysis of a class of empirical design techniques for probe-fed, U-slot microstrip patch antennas," *IEEE Trans. Antennas Propag.*, vol. 64, no. 7, pp. 2758–2770, Jul. 2016.

[24] F. A. Dicandia and S. Genovesi, "Characteristic modes analysis of non-uniform metasurface superstrate for nanosatellite antenna design," *IEEE Access*, vol. 8, pp. 176050–176061, 2020.

[25] J. Zeng, X. Liang, L. He, F. Guan, F. H. Lin, and J. Zi, "Single-fed triple-mode wideband circularly polarized microstrip antennas using characteristic mode analysis," *IEEE Trans. Antennas Propag.*, vol. 70, no. 2, pp. 846–855, Feb. 2022.

[26] A. Sharma, D. Gangwar, R. P. Singh, R. Solanki, S. Rajpoot, B. K. Kanaujia, S. P. Singh, and A. Lay-Ekuakille, "Design of compact wideband circularly polarized hexagon-shaped antenna using characteristics mode analysis," *IEEE Trans. Instrum. Meas.*, vol. 70, pp. 1–8, 2021.

[27] H. Wang, Y. B. Park, and I. Park, "Low-profile wideband solar-cell-integrated circularly polarized CubeSat antenna for the Internet of Space Things," *IEEE Access*, vol. 10, pp. 61451–61462, 2022.

[28] H. H. Tran, N. Nguyen-Trong, and H. C. Park, "A compact dual circularly polarized antenna with wideband operation and high isolation," *IEEE Access*, vol. 8, pp. 182959–182965, 2020.

[29] C. A. Balanis, *Antenna Theory Analysis and Design*, 3rd ed. Hoboken, NJ, USA: Wiley, 2005.

[30] A. Sakonkanapong and C. Phongcharoenpanich, "Near-field HF-RFID and CMA-based circularly polarized far-field UHF-RFID integrated tag antenna," *Int. J. Antennas Propag.*, vol. 2020, pp. 1–15, Apr. 2020.

[31] *IEEE Standard Test Procedures for Antennas*, ANSI/IEEE Standard 149-1979, Nov. 1979, pp. 1–144.

[32] A. Kumar and R. Mittra, "Gain and side lobe level enhancement of array antennas using metasurface superstrates," in *Proc. IEEE Int. Symp. Antennas Propag. USNC/URSI Nat. Radio Sci. Meeting*, Jul. 2018, pp. 1503–1504.

[33] B. K. Lau and Y. H. Leung, "A Dolph-Chebyshev approach to the synthesis of array patterns for uniform circular arrays," in *Proc. IEEE Int. Symp. Circuits Syst. (ISCAS)*, Geneva, Switzerland, May 2000, pp. 124–127.

[34] M. A. Sarker, M. S. Hossain, and M. S. Masud, "Robust beamforming synthesis technique for low side lobe level using Taylor excited antenna array," in *Proc. 2nd Int. Conf. Electr., Comput. Telecommun. Eng. (ICECTE)*, Rajshahi, Bangladesh, Dec. 2016, pp. 1–4.

[35] A. Nešić, I. Radnović, and Z. Mićić, "Printed antenna arrays with high side lobe suppression," *Act. Passive Electron. Compon.*, vol. 2008, pp. 1–6, Jan. 2008.

[36] G. Sun, Y. Liu, H. Li, S. Liang, A. Wang, and B. Li, "An antenna array sidelobe level reduction approach through invasive weed optimization," *Int. J. Antennas Propag.*, vol. 2018, pp. 1–16, Jan. 2018.

[37] O. K. Eyiogwu, "The issue of sidelobe level in antenna array: The challenge and the possible solution," in *Antenna Arrays—Applications to Modern Wireless and Space-Born Systems*. London, U.K.: IntechOpen, Nov. 2022.

[38] K. L. Chung, S. Chaimool, and C. Zhang, "Wideband subwavelength-profile circularly polarised array antenna using anisotropic metasurface," *Electron. Lett.*, vol. 51, no. 18, pp. 1403–1405, 2015.

[39] S. Liu, D. Yang, and J. Pan, "A low-profile broadband dual-circularly-polarized metasurface antenna," *IEEE Antennas Wireless Propag. Lett.*, vol. 18, no. 7, pp. 1395–1399, Jul. 2019.

[40] N. Hussain, M. Jeong, A. Abbas, T. Kim, and N. Kim, "A metasurface-based low-profile wideband circularly polarized patch antenna for 5G millimeter-wave systems," *IEEE Access*, vol. 8, pp. 22127–22135, 2020.

[41] P. K. Rajanna, K. Rudramuni, and K. Kandasamy, "Characteristic mode-based compact circularly polarized metasurface antenna for in-band RCS reduction," *Int. J. Microw. Wireless Technol.*, vol. 12, no. 2, pp. 131–137, Sep. 2019.

[42] Q. Chen, G. Zhang, C. He, Y. Fan, Z. Zhu, D. Zhang, J. Li, and Y. Zhao, "Wideband and high-gain circularly-polarized L-shaped slot antenna array using metamaterial," *Int. J. Microw. Wireless Technol.*, vol. 13, no. 4, pp. 359–364, Jul. 2020.

[43] W. He, Y. He, S.-W. Wong, L. Zhang, W. Li, H. Cui, and A. Boag, "A low-profile ultra-wideband circularly polarized antenna array with metasurface," *Int. J. RF Microw. Comput.-Aided Eng.*, vol. 13, no. 12, Aug. 2021, Art. no. e22874.

[44] J. Dong, C. Ding, and J. Mo, "A low-profile wideband linear-to-circular polarization conversion slot antenna using metasurface," *Materials*, vol. 13, no. 5, p. 1164, Mar. 2020.

[45] W. Yang, Q. Meng, W. Che, L. Gu, and Q. Xue, "Low-profile wideband dual-circularly polarized metasurface antenna array with large beamwidth," *IEEE Antennas Wireless Propag. Lett.*, vol. 17, no. 9, pp. 1613–1616, Sep. 2018.

[46] S. X. Ta and I. Park, "Compact wideband circularly polarized patch antenna array using metasurface," *IEEE Antennas Wireless Propag. Lett.*, vol. 16, pp. 1932–1936, 2017.

[47] T. T. Le, H. H. Tran, and A. A. Althuwayb, "Wideband circularly polarized antenna based on a non-uniform metasurface," *Appl. Sci.*, vol. 10, no. 23, p. 8652, Dec. 2020.

[48] J. A. Sheersha, N. Nasimuddin, and A. Alphones, "A high gain wideband circularly polarized antenna with asymmetric metasurface," *Int. J. RF Microw. Comput.-Aided Eng.*, vol. 29, no. 7, Mar. 2019, Art. no. e21740.

[49] S. X. Ta and I. Park, "Planar wideband circularly polarized metasurface-based antenna array," *J. Electromagn. Waves Appl.*, vol. 30, no. 12, pp. 1620–1630, 2016.

[50] S.-X. Ta and I. Park, "Low-profile broadband circularly polarized patch antenna using metasurface," *IEEE Trans. Antennas Propag.*, vol. 63, no. 12, pp. 5929–5934, Dec. 2015.

NATHAPAT SUPREEYATITIKUL (Member, IEEE) received the B.Eng. degree from Mahidol University, Thailand, in 2014, the M.Eng. degree from the King Mongkut's University of Technology Thonburi (KMUTT), Thailand, in 2016, and the D.Eng. degree from the King Mongkut's Institute of Technology Ladkrabang (KMITL), Thailand, in 2022. His research interests include circularly polarized antennas and MIMO antennas.

PISIT JANPANGNGERN was born in Lampang, Thailand, in 1991. He received the B.Eng. degree from the Rajamangala University of Technology Thanyaburi, Thailand, in 2015, and the M.Eng. degree from the King Mongkut's Institute of Technology Ladkrabang (KMITL), Thailand, in 2017, where he is currently pursuing the D.Eng. degree. His research interest includes omnidirectional circularly polarized antennas.

TITIPONG LERTWIRIYAPRAPA (Senior Member, IEEE) received the B.S.Tech.Ed. degree in electrical engineering from the King Mongkut's University of Technology North Bangkok, in 1996, the M.Eng. degree in electrical engineering from the King Mongkut's Institute of Technology Ladkrabang, in 2000, and the M.Sc. and Ph.D. degrees in electrical engineering from The Ohio State University, Columbus, OH, USA, in 2006 and 2007, respectively. He is currently an Associate Professor with the Department of Teacher Training in Electrical Engineering, King Mongkut's University of Technology North Bangkok. His research interests include electromagnetic theory, metamaterial, asymptotic, computational electromagnetics, and hybrid methods. He received the third place in the 2007 USNC/CNC URSI Student Paper Competition, Ottawa, Canada; and the Best Paper Award from the 2008 International Symposium on Antennas and Propagation (ISAP2008), Taiwan. He was at the Board Committee of the ECTI Association, from 2012 to 2015.

MONAI KRAIRIKSH (Senior Member, IEEE) was born in Bangkok, Thailand. He received the B.Eng., M.Eng., and D.Eng. degrees in electrical engineering from the King Mongkut's Institute of Technology Ladkrabang (KMITL), Thailand, in 1981, 1984, and 1994, respectively. He was a Visiting Research Scholar at Tokai University, in 1988, and the Communications Research Laboratory (CRL), Yokosuka Radio Communications Research Center, in 2004. He worked as the Director of the Research Center for Communications and Information Technology, from 1997 to 2002. He joined the KMITL, where he is currently a Professor with the Department of Telecommunication Engineering. His main research interests include antennas for wireless communications and microwave in agricultural applications. He was recognized as a Senior Research Scholar of the Thailand Research Fund, in 2005 and 2008, and a Distinguished Research Scholar of the National Research Council of Thailand. He served as a Distinguished Lecturer for the IEEE Antennas and Propagation Society, from 2012 to 2014. He was the Chairperson of the IEEE MTT/AP/Ed Joint Chapter, in 2005 and 2006. He served as the General Chairperson of the 2007 Asia-Pacific Microwave Conference, and the Advisory Committee of the 2009 International Symposium on Antennas and Propagation. He was the President of the Electrical Engineering/Electronics, Computer, Telecommunications and Information Technology Association (ECTI), in 2010 and 2011, and the Editor-in-Chief of the *ECTI Transactions on Electrical Engineering, Electronics, and Communications*.

CHUWONG PHONGCHAROENPANICH (Member, IEEE) received the B.Eng. (Hons.), M.Eng., and D.Eng. degrees from the King Mongkut's Institute of Technology Ladkrabang (KMITL), Bangkok, Thailand, in 1996, 1998, and 2001, respectively. He is currently a Professor with the Department of Telecommunications Engineering, KMITL, where he also serves as the Leader for the Innovative Antenna and Electromagnetic Applications Research Laboratory. His research interests include antenna design for various mobile and wireless communications, conformal antennas, and array antenna theory. He is a Senior Member of IEICE and a member of ECTI. He has been on Organizing Committee of several international conferences, including the TPC Chair of 2009 International Symposium on Antennas and Propagation (ISAP 2009) and a TPC Member of ISAP 2012. He was on the Board Committee of ECTI Association, from 2008 to 2011 and from 2014 to 2015. He has served as the Chair for the IEEE MTT/AP/ED Thailand Chapter, from 2014 to 2018. He is also a Reviewer of many scientific journals, including the IEEE TRANSACTIONS ON ANTENNAS AND PROPAGATION, IEEE ACCESS, *IET Microwaves, Antennas and Propagation Electronics Letters*, *ECTI Transactions*, and many international conferences, including ISAP and APMC. He was an Associate Editor of the *IEICE Transactions on Communications* and the *ECTI Transactions on Electrical Engineering, Electronics, and Communications*. He is also an Associate Editor of the *IEICE Communications Express*.